

# Benzimidazole–Piperazine–Coumarin/Cucurbit[7]uril Supramolecular Photoinduced Electron Transfer Fluorochromes for Detection of Carnosol by Stimuli-Responsive Dye Displacement and $pK_a$ Tuning

Rukayat S. Bojesomo, Khaleel I. Assaf, Haythem A. Saadeh, Lamia A. Siddig, and Na'il Saleh\*

Cite This: *ACS Omega* 2022, 7, 2356–2363

Read Online

ACCESS |



Metrics &amp; More

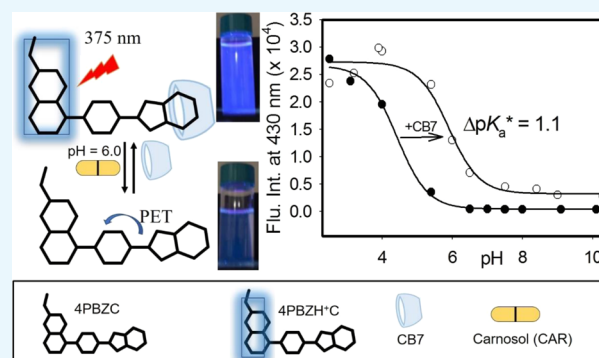


Article Recommendations



Supporting Information

**ABSTRACT:** A new fluorescent dye (4PBZC) comprising coumarin (C), piperazine (P), and benzimidazole (BZ) was designed, prepared, and complexed to cucurbit[7]uril (CB7) to detect carnosol (CAR), an anti-breast cancer drug, in sub-nanomolar concentrations utilizing the supramolecular indicator displacement assay strategy, the CB7-assisted  $pK_a$  shift, and the CB7-retarded photoinduced electron transfer process. The host–guest complexation was confirmed by UV–visible absorption, fluorescence, and  $^1\text{H}$  NMR spectroscopy, which established the binding of 4PBZC to CB7. CB7 preferentially binds the indicator dye (4PBZC) via the protonated BZ residue compared to the neutral BZ one, demonstrated by a higher binding constant of the complex in its di-protonated form, which led to an increase in the  $pK_a$  of the BZ moiety by ca. 3.0 units after the addition of CB7. In aqueous solution (pH 6), switching the emission signals between 4PBZH<sup>+</sup>C/ CB7 (ON state) and 4PBZC (OFF state) was achieved by displacement of the protonated dye from the cavity of CB7 by the CAR analyte. An efficient sensor was obtained for the sensitive detection of CAR in aqueous solution with a low detection limit of 0.148 ng/mL (0.45 nM) and a linear range from 20 to 627 ng/mL.



## 1. INTRODUCTION

In recent years, the number of indicator displacement assays (IDAs)<sup>1</sup> has increased dramatically as an eminent strategy for changing a synthetic receptor (host) into an optical sensor. In a conventional IDA, an indicator (dye) is first permitted to reversibly bind a host, before being dislodged from the host with a competitive analyte (e.g., drug), and thus, the strategy regulates an optical signal despite that the analyte and the host are both optically inactive. It is quite crucial that the indicator and analyte have a similar binding affinity for the receptor in order to achieve a high sensitivity.<sup>2–6</sup> The IDA principle depends on the relocation of the dye from the hydrophobic cavity of the host into the bulk upon the addition of a competitor analyte. The host–dye inclusion complex has distinctive optical properties, which differ from those of the uncomplexed dye, and therefore, the displacement of the dye with a competitor analyte results in a signal in relation to the concentration of the analyte.<sup>7</sup> This differs from the associative binding assay (ABA), where both the dye and the analyte are entrapped into the cavity of the host. ABA empowers the discovery and separation of analytes through developing spectroscopic fingerprints because of dye–analyte correspondences.<sup>2</sup>

The employment of cucurbit[*n*]urils (CBs)<sup>8</sup> to tweak fluorescence signals utilizing the IDA strategy is well-known for detection of spectroscopically (optically) silent drug molecules.<sup>9–13</sup> The reported sensing strategies in these examples were conceivably dependent on numerous processes, such as the host-assisted interactions between aromatic rings,<sup>9–11</sup> the host-assisted aggregation-induced emission (AIE),<sup>12</sup> or the dye deaggregation upon complexation.<sup>13</sup> The utilization of other beneficial chemical equilibria and photochemical processes, which lead to the generation of fluorescent sensors that are highly sensitive to the analyte, has yet to be reported.

Compared to cyclodextrins (CDs), CBs have distinct advantages in that they can modulate the acid–base equilibrium of the encapsulated guest molecule without changing the pH of the media due to ion–dipole interactions

Received: November 8, 2021

Accepted: December 17, 2021

Published: January 5, 2022



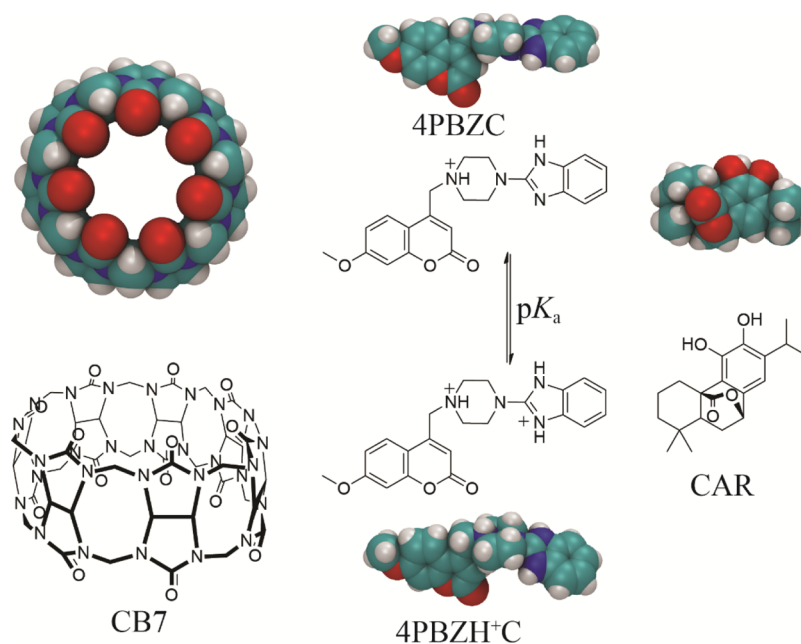


**Figure 1.** Molecular structure of CB7, fluorescent probe (4PBZC, in the mono- and di-protonated forms), and CAR.

between the positive center of the guest molecule and the carbonyl groups of CB.<sup>8,14</sup> CBs are also known for their ultrahigh binding affinities as a host toward a guest molecule in aqueous medium compared to other macrocycles such as CDs.<sup>8</sup> Because of these distinct hosting properties, particularly being non-toxic (in the low-mM range) *in vivo* and *in vitro*,<sup>15,16</sup> CBs have been widely used to increase the aqueous solubility of drug molecules<sup>17</sup> such as benzimidazole (BZ)<sup>18</sup> and benzothiazole (BT) derivatives<sup>19,20</sup> and to develop supramolecular IDA assay for the detection of over-the-counter drugs<sup>21–25</sup> and steroids.<sup>26</sup> Specifically, the distinct host-induced  $pK_a$  shifts of CB have already been exploited for the development of new chemical sensors through monitoring the fluorescence changes upon the competitive displacement of the dye molecule from the cavity of the host with important drug molecules, such as cadaverine<sup>2,27</sup> and osterotides.<sup>28</sup>

Aside from host-assisted  $pK_a$ , the affinity of CB toward cationic guest molecules was exploited by our research group<sup>19</sup> to demonstrate the potential usefulness of CBs for the suppression of the photoinduced electron transfer (PET) process through the effective protonation of the encapsulated guest molecules without changing the pH of the media. PET reactions are ubiquitous in both chemistry and biology. It involves the transfer of an electron from a donor unit to an acceptor unit and can occur photochemically.<sup>29</sup> Fabrication of fluorescent IDA-based sensors, which combines the CB-controlled PET and complexation-induced  $pK_a$  shift, is particularly motivated because they impart high sensitivity.

Herein, a new fluorescent probe was designed (4PBZC, Figure 1) to reversibly switch on and off its emission in response to the anti-breast cancer carnosol (CAR, Figure 1), which is optically transparent. In general, PET fluorophores are designed and synthesized based on the potential usefulness of their electron-donating and electron-accepting groups and their biocompatibility. The design is based on the combination of three residues: coumarin (C) as a fluorophore, piperazine (P) as a spacer, and BZ as a cavity binder. These bioactive moieties are known to have affinities for cucurbit[7]uril (CB7,

Figure 1)<sup>20,30,31</sup> and were used to generate sensors with reversal fluorescent response to several analytes utilizing the PET process,<sup>32,33</sup> which rationalizes their selection. The BT in the previously reported probe 4PBTC<sup>19</sup> is particularly replaced here with the more basic BZ group to shift the sensing pH from 3 to 6. More importantly, the new supramolecular IDA-based sensor 4PBZC operates based on both the CB7-assisted  $pK_a$  shift and the CB7-retarded PET process to develop a highly sensitive sensor for CAR with a low detection limit (LOD) in nanomolar concentration under physiological pH.

## 2. RESULTS AND DISCUSSION

**2.1. Interaction of 4PBZC with CB7 in Aqueous Solution: CB7-Induced  $pK_a$  Shifts.** The evolution of the UV–visible absorption spectra of the probe 4PBZC (35  $\mu\text{M}$ ) and its complex with CB7 (500  $\mu\text{M}$ ) was studied as a function of HCl inputs in aqueous medium (Figures 2 and S1). In general, the absorption spectra of 4PBZC and 4PBZC/CB7 showed two main bands that exhibited a drastic increase and shift (from 285 and 325 to 280 and 335 nm, respectively) when pH was decreasing from 9 to 3 upon the addition of HCl

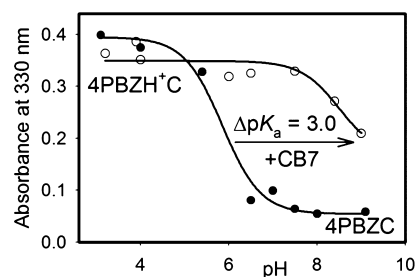


**Figure 2.** Titration plots of the UV–visible absorbance at 330 nm of the probe 4PBZC (35  $\mu\text{M}$ ) as a function of pH from 2 to 10 in the absence of CB7 (filled circles) and in the presence of 500  $\mu\text{M}$  ( $\sim 14$  equiv to ensure complexation at high pH values) of CB7 (empty circles). The corresponding Henderson–Hasselbalch sigmoidal fits (see the Experimental Section) are also shown.

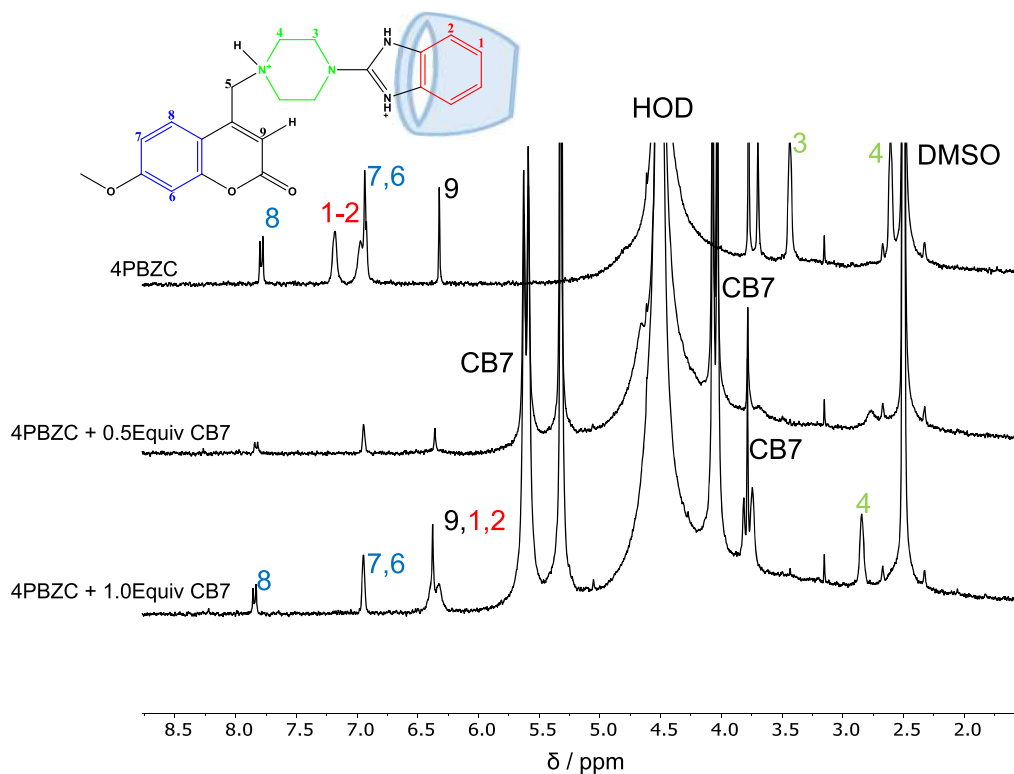


**Figure 3.**  $^1\text{H}$  NMR spectra (400 MHz, 50%  $\text{DMSO-}d_6$  and 50%  $\text{D}_2\text{O}$ ) of 4PBZC (1 mM) in the absence (free) and presence of 0.5 and 1.0 equiv of CB7 298 K and pD 7.

(see the [Supporting Information](#) for details). The acid dissociation constant ( $\text{p}K_a$ ) with respect to the protonation and deprotonation of the nitrogen atom in the BZ unit of 4PBZC ([Figure 1](#)) was determined by fitting the corresponding pH titration plots to sigmoidal functions.<sup>19</sup> The shift in the  $\text{p}K_a$  value by ca. 3.0 units (from  $5.8 \pm 0.1$  to  $8.8 \pm 0.1$ ) in the presence of CB7 confirms the formation of a host–guest complex of CB7 with the di-protonated form (4PBZH<sup>+</sup>C) preferentially over the mono-protonated 4PBZC, which reflects the difference in the binding affinity of CB7 toward the di-protonated (pH 3) and mono-protonated forms (pH 9) of the indicator dye. The UV–visible titrations indicated the formation of a 2:1 host–guest complex for CB7/4PBZH<sup>+</sup>C with a stability constant of  $5.5 \times 10^6 \text{ M}^{-2}$  at pH 3 ([Figure S3](#)). In contrast, very low binding affinity of the mono-protonated with CB7 was noticed from the corresponding binding UV titration data at pH 9; see the [Supporting Information](#) for details on all the corresponding binding titrations using UV–visible absorption spectra.

The type of interaction, stoichiometry, and mode of inclusion were investigated at pH (pD) 7 using NMR spectroscopy, as shown in [Figure 3](#). Upon the addition of 1 molar equivalent of CB7 to a solution of 4PBZC, two proton resonances H-1 and H-2 corresponding to the BZ unit were shifted to lower ppm values with approximately 0.95 ppm, signifying their encapsulation into the hydrophobic cavity of CB7, while two resonance protons of the C unit, H-3 and H-4, were slightly shifted to higher ppm (from 3.69 and 2.59 to 3.80 and 2.81 ppm, respectively), which attributed to their position near the carbonyl portal. The  $^1\text{H}$  NMR binding titration was also conducted at a pH (pD) of  $\sim 3$ . The results indicated the possible formation of a 2:1 host–guest complex in agreement with the UV–visible titrations; see the [Supporting Information](#)

for details on all the corresponding binding titrations using  $^1\text{H}$  NMR spectroscopy.

Density functional theory (DFT) calculations were performed in the gas phase to shed light on the structure of the host–guest complexes and evaluate their binding energy. Several starting geometries were considered for the structural optimization, which include the formation of inclusion 4PBZC/CB7 complexes either through the entrapment of the BZ residue inside the cavity of CB7 or through the C moiety (see the [Supporting Information](#) when both units are entrapped inside CB7). The optimized structures are shown in [Figure 4](#). The DFT-calculated structure showed that both BZ and C can be complexed inside the cavity of CB7 in both the mono- and di-protonated forms. In addition, the calculated interaction energy revealed that the 4PBZH<sup>+</sup>C binds more tightly than the corresponding 4PBZC, which is in line with the additional stabilization through ion–dipole interactions and in agreement with the NMR results.

**2.2. Supramolecular Effects on Fluorescence: CB7-Assisted Apparent  $\text{p}K_a^*$  Shifts.** The empirical excited-state dissociation constant ( $\text{p}K_a^*$ ) associated with the mono- and di-protonated equilibrium of the nitrogen atom in the BZ unit of 4PBZC was determined by pH titration using fluorescence spectroscopy ([Figure 5](#)). The apparent  $\text{p}K_a^*$  shift of ca. 1.1 unit (from 4.7 to 5.8) due to the formation of a host–guest inclusion complex between CB7 and the indicator dye (see NMR results) manifests a significant difference in the binding affinities of CB7 toward the di-protonated and mono-protonated forms because of the ion–dipole interactions between the protonated BZ unit and the carbonyl groups at the portal of the cavity (see the [Supporting Information](#) for the corresponding spectra to the plots in [Figure 5](#) and the binding titration by fluorescence spectroscopy).

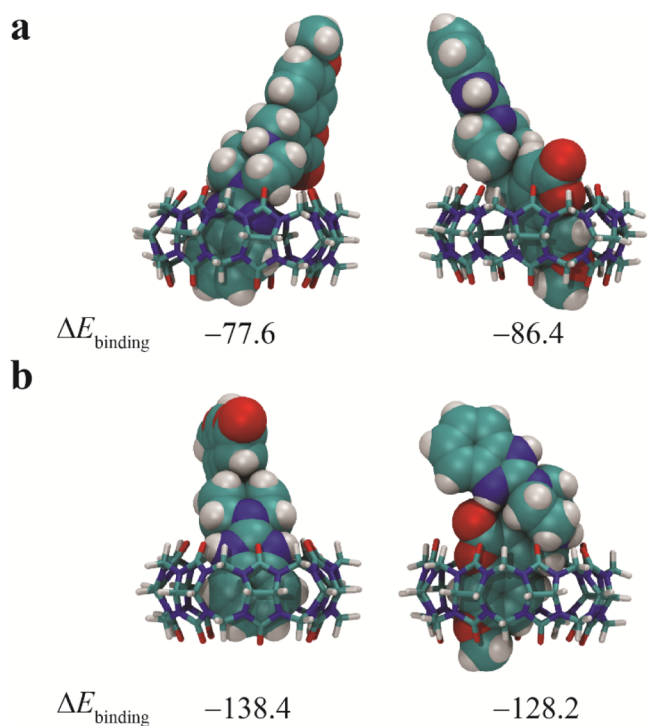


**Figure 4.** DFT-optimized structures of (a) CB7/4PBZC and (b) CB7/4PBZH<sup>+</sup>C, considering the complexation through the BZ (left) or C (right) units. The corresponding binding energies are given in kcal/mol.

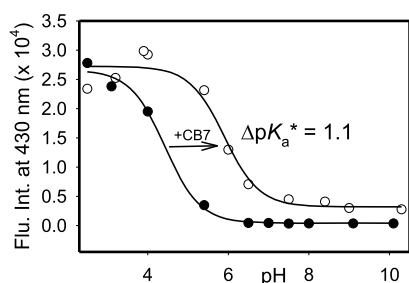


**Figure 5.** Host-induced  $pK_a^*$  shift of probe 4PBZC (35  $\mu\text{M}$ ) studied by pH titration from pH 2 to pH 10 in the absence of CB7 (filled circles) and presence of 500  $\mu\text{M}$  of CB7 (empty circles) at an excitation wavelength of 375 nm.

The observed  $pK_a^*$  value for the complex at the excited state is smaller than the determined  $pK_a$  value at the ground state, which confirms the need to consider the photoacidity of the complex when estimating its  $pK_a$  value.<sup>34</sup> Although retrieving the true  $pK_a^*$  value upon the addition of CB7 is beyond the focus of the present study, the plots in Figure 5 underline the pH value at which one could best utilize the host-induced turnover in the emission intensity of the indicator dye when employing the supramolecular IDA, at a pH of around 5.8. Encouraged by the neutrality of BZ and C units and their biological applications, we opted for pH 6 to develop our sensing method for CAR (see below).

**2.3. Mechanism of Fluorescence Turnover: CB7-Retarded PET.** In the mono-protonated form, the fluorescence is quenched by the PET, where the lone-pair electrons on the heteroatoms (e.g., amine group in the BZ) are of higher energy than the highest occupied molecular orbital (HOMO) of the fluorophore (i.e., coumarin). Upon

excitation of an electron from the HOMO to the lowest unoccupied molecular orbital (LUMO) of the fluorophore, the lone-pair electrons drop down to the partially empty HOMO of the fluorophore; this prevents the excited electron from returning to the fluorophore HOMO and accordingly results in quenching of the fluorescence. In contrast, the protonation of the amine group lowers the energy of the lone-pair state below that of the fluorophore HOMO, which will, therefore, prevent the quenching process and restore the fluorescence. DFT calculations indicated that the HOMO orbitals for 4PBZC are positioned on the BZ and P, while the LUMO orbitals are located at the C unit (Figure S10). In contrast, for 4PBZH<sup>+</sup>C, the HOMO orbitals mostly reside on the C part, and LUMO orbitals are positioned on the BZ and P units. The suppression of the PET process by the addition of CB7 at pH 6 due to the host-assisted protonation led to a significant emission enhancement (Figure S11a). The absorption band at the red side, which belongs to the di-protonated form, was also restored upon the addition of CB7 at pH 6 (Figure S11b). At pH 6, the BZ unit is neutral, but when leached into the cavity of CB7, host–guest ion–dipole interactions protonate the ring and suppress the intramolecular PET process, restoring the emission coming from the coumarin unit. Very significant changes were noticed, which highlights the distinct advantage of one of our adopted sensing strategies.

Collectively, the theoretical results confirm that the intramolecular PET takes place from the neutral BZ to the C unit, which can subsequently be suppressed by different inputs such as H<sup>+</sup> or CB7 macromolecules, among others. Experimentally, the suppression of the PET process by the addition of HCl (Figures S6 in the Supporting Information) or CB7 at pH 6 because of the host-assisted protonation led to a significant emission enhancement (Figure S11 in the Supporting Information).

**2.4. Supramolecular IDA for CAR and Fluorescence Standard Sensing Curves.** To investigate the competitive displacement of the dye from the cavity of the host by CAR drug, we started with the 4PBZH<sup>+</sup>C/CB7 complex at pH 6, at which the complexed dye exists in its di-protonated form, whereas the free form of the indicator dye remains in its mono-protonated, non-emissive form in the ground (Figure 2) or excited states (Figure 5) because of intramolecular PET reaction. The displacement was followed using UV–visible absorption and fluorescence spectroscopy (Figure 6) in aqueous solution at pH 6. Although, excess concentration of CB7 was used to ensure full complexation to the dye before adding CAR, the displacement titration revealed an evident response at low CAR concentrations. The excitation wavelength was selected at 375 nm to selectively excite the C fluorophore and avoid any interference from the BZ. Addition of CAR has caused the expected evolution of the spectral profiles pertinent to the mono-protonated form in that the absorption band at about 335 nm shifts back to the blue region (325 nm) with a concomitant decrease in fluorescence intensity (Figure 6a,c). These significant spectral changes confirmed the complexation of CAR with CB7 at the expense of displacing the BZ unit from the cavity of CB7 gradually with the increase in its concentration. The binding of CAR to CB7 was further confirmed by <sup>1</sup>H NMR experiment (Figure S12). It should be noted that the cavity size of CB7 (242 Å<sup>3</sup>) is insufficient to allow the complexation of both the BZ and CAR (formation of the ternary complex); thus, only dye displacement is possible.

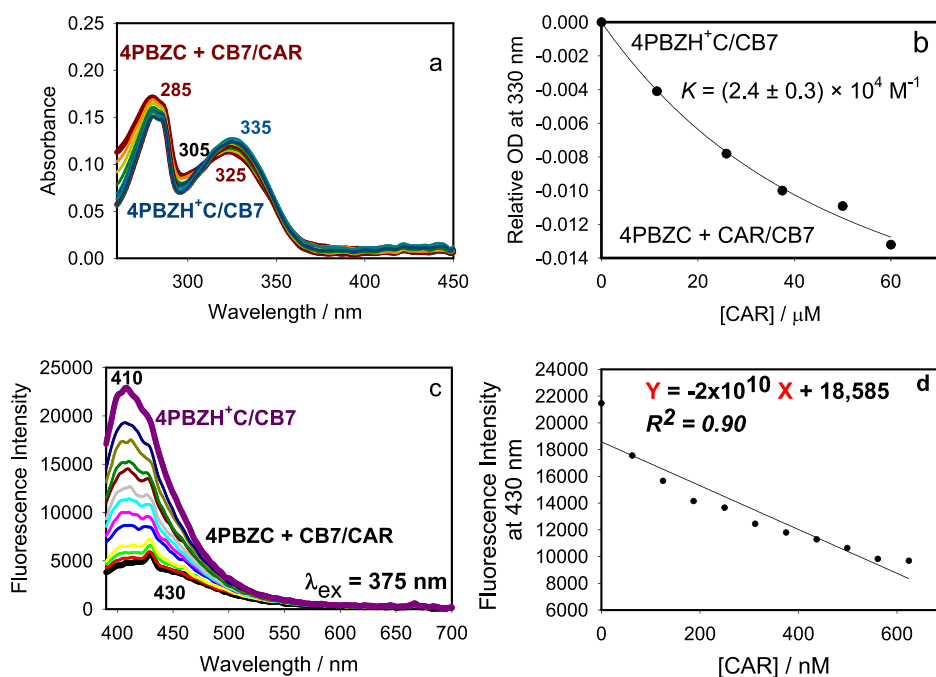


**Figure 6.** Changes in the UV–visible absorbance (a) and fluorescence (c) spectra of the CB7-complexed dye (15  $\mu\text{M}$  + 1 mM) upon the addition of CAR at different concentrations in aqueous solution at pH 6 and 298 K. The non-linear fit ( $K$  reported as an apparent binding constant) of absorbance data (b) to a 1:1 binding model (solid line and the Experimental Section) and the linear fit (d) of the fluorescence data are also shown. The change in optical density ( $\Delta\text{OD}$ ) is the difference between the absorbance in the absence and presence of CB7.

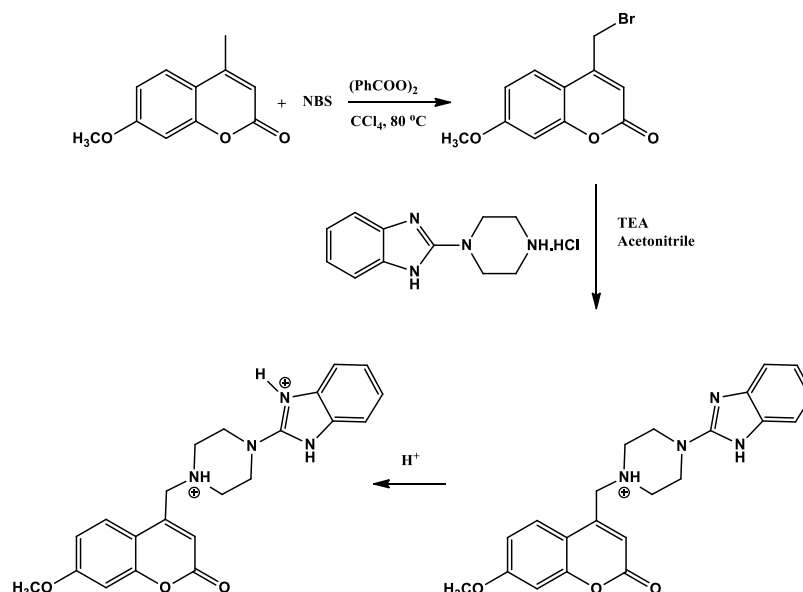
**Table 1. Comparison of Detection Limits with Other Proposed Dyes of Recent Sensing Methods for the Detection of CAR and Other Spectroscopically Silent Drugs**

dye	guest	host	binding affinity, $K$	LOD	method	refs
ABAM	amantadine	CB7	$8.7 \times 10^8$	0.35 nM	IDA	11
TPPE	methamphetamine	CB7	$\sim 108$	$0.43 \mu\text{M}$	AIE	12
palmatine	methotrexate	CB7		$0.03 \mu\text{M}$	IDA	10
berberine	methotrexate	CB7		$0.06 \mu\text{M}$	IDA	10
coptisine	methotrexate	CB7		$0.13 \mu\text{M}$	IDA	10
palmatine	phenylalanine	CB8	$1.0 \times 10^5$		IDA	9
berberine	dibucaine	CB7	$9.6 \times 10^4$	6.0 nM	IDA	39
palmatine	dibucaine	CB7	$4.3 \times 10^4$	12.0 nM	IDA	39
coptisine	dibucaine	CB7	$1.9 \times 10^5$	25.0 nM	IDA	39
MPCP	memantine	CB8	$\sim 1012$		IDA	6
4PBZC	CAR	CB7	$2.4 \times 10^4$	0.45 nM	IDA + PET + pKa shifts	this work
CdSe/ZnS QDs	CAR	graphene		$>0.7 \mu\text{M}$	electrochemical sensing	40

Detection of CAR is of high medical value. CAR is a polyphenolic diterpene compound found in herbs such as rosemary (*Rosmarinus officinalis*). As a derivative of carnosic acid,<sup>35</sup> CAR has been proven to be an effective anti-inflammatory, antioxidant, antimicrobial, and anti-cancer agent.<sup>36</sup> Encapsulation of CAR and carnosic acid by a macrocyclic compound such as  $\alpha$ ,  $\beta$ , and  $\gamma$ -CD was reported.<sup>37</sup> Park et al. discovered an enhancement in antioxidant and antimicrobial properties of carnosic acid, with respect to the increase in its solubility resulting from encapsulation into the cavity of  $\beta$ -CD.<sup>38</sup> The fascinating point to be broached here is that the exploitation of CB7-induced  $\text{p}K_a$  shift (when compared to CDs) allowed us to shift the sensing pH to what could best meet the criteria demanded for sensing CAR under or near physiological conditions. This coupled with the utilization of host-suppressed PET enabled us to extend the linearity of our detection for very low concentrations of CAR. Specifically, the obtained linear range and LOD by our method

were 20 to 207 and 0.15 ng/mL (0.45 nM), respectively (Figure 6d).

The high sensitivity of the present sensor highlights the importance of our newly designed sensing technology and its superiority when compared to other reports for detections of CAR (less than  $0.7 \mu\text{M}$ )<sup>40</sup> and other spectroscopically silent drugs (Table 1). For example, in early studies, an effective dye was designed based on the carbazole moiety to switch on and off the fluorescence signals in response to the addition of cadaverine through the employment of CB6-assisted guest protonation.<sup>27</sup> Also, CB8-encapsulated acridine dye was applied for the fluorescent detection of the peptide drug octreotide in aqueous solution utilizing the competitive host-assisted  $\text{p}K_a$  shift.<sup>41</sup> However, more recently, although IDA-driven sensing of amantadine drug with an anthracyclic-based probe (ABAM) in the presence of CB7 resulted in quenching of the emission of the probe with a recorded LOD of 0.35 nM,<sup>11</sup> the dibucaine drug sensed by quenched emission of

Scheme 1. Synthetic Route for 4PBZC and 4PBZH<sup>+</sup>C

berberine, palmatine, and coptisine dyes gave a LOD of 6.0, 12.0, and 25.0 nM, respectively,<sup>39</sup> while emission of the TPPE/CB7 complex enhanced with the addition of methamphetamine as a result of aggregate-induced emission produced a LOD of only 0.43  $\mu\text{M}$ .<sup>12</sup> Furthermore, Alzheimer disease drug “memantine” was sensed in the blood serum through the IDA mechanism with [2.2]paracyclophane-derivative-indicator dyes and CB8 as a macrocycle.<sup>6</sup> Moreover, in the recent determination of the amino acid phenylalanine<sup>9</sup> and the anticancer drug methotrexate<sup>10</sup> by the palmatine/CB7 complex, the fluorescence signal of the indicator palmatine dye was enhanced inside CB7 because of the host-assisted extended conjugation between the two rings in the structure of palmatine: the isoquinoline and the substituted benzene rings. When the drug replaced the dye from the cavity of CB7, fluorescence was subsequently quenched with yet reported LOD in  $\mu\text{M}$  concentrations.

### 3. CONCLUSIONS

A new fluorescent molecule (4PBZC) was designed to develop a new sensing approach for CAR and potentially other drug analytes. The method in the present study was demonstrated to have superior sensitivity when compared to other analytical methods that utilize other fluorescent sensing mechanisms for the detection of drug molecules. In our approach, we have distinctly relied on the combination of three supramolecular effects: IDA, host-retarded PET, and host-induced  $pK_a$  shifts. The former allows us to sense optically inert drugs, the second allows us to generate nanomolar sensitivity, and the later allows us to control the sensing pH and shift its value toward the physiological range. Altogether, the developed approach by simultaneous integration of three concepts has been best utilized for the detection of CAR yet can also be utilized toward detections of other prospective drugs or some relevant biomedical and analytical applications.

### 4. EXPERIMENTAL SECTION

**4.1. Chemicals.** Coumarin, CAR, BZ, piperazine (highest purity), and CB7 (with 25% water content) were bought from Sigma-Aldrich ([www.sigmaaldrich.com](http://www.sigmaaldrich.com)) and utilized as re-

ceived. Deuterated solvents ( $\text{D}_2\text{O}$ ) were additionally bought from Sigma-Aldrich (99.9 atom % D).

**4.2. Synthesis of the 4PBZC Probe (4-((4-(1H-Benzo[d]imidazole-2-yl)piperazin-1-yl)methyl)-7-methoxy-2H-chromen-2-one).** To a mixture of 7-methoxy-4-methylcoumarin (1 mmol) and NBS (1.1 mmol) in  $\text{CCl}_4$  (15 mL), a catalytic amount of benzoyl peroxide was added. The reaction mixture was refluxed for 8 h, and after cooling, the succinimide produced during the reaction was filtered off, and the solvent was washed with  $\text{H}_2\text{O}$ , dried, and removed under reduced pressure. The crude product was pure enough and used as is for the next step.

A solution of 4-bromomethyl-7-methoxycoumarin (1 mmol), 2-(piperazin-1-yl)-1H-benzo[d]imidazole (1.1 mmol), and triethylamine (4 mmol) in 10 mL of dry acetonitrile was stirred overnight at room temperature. After completion, the solvent was removed under vacuum, dissolved in ethyl acetate (25 mL), and then washed with water. The organic layer was dried over anhydrous sodium sulfate, the solvent was evaporated, and the crude was crystallized from ethyl acetate/hexane to give pure 4-((4-(1H-benzo[d]imidazole-2-yl)piperazin-1-yl)methyl)-7-methoxy-2H-chromen-2-one (4PBZC). White solid, 70% yield, mp 216–217 °C. <sup>1</sup>H NMR (400 MHz, DMSO):  $\delta$  3.9 (s, 1H), 8.00 (d,  $J$  = 8 Hz, 1 H),  $\delta$  7.18 (m, 2H), 7.04 (m, 3H), 6.89–6.86 (m, 2H), 3.89 (s, 2H), 3.76 (s, 3H), 3.41 (t,  $J$  = 8 Hz, 4H), 2.67 (t,  $J$  = 8 Hz, 4H) ppm. <sup>13</sup>C NMR:  $\delta$  162.703, 160.732, 156.403, 155.846, 143.670, 143.647, 134.449, 127.304, 126.963, 120.780, 112.521, 112.439, 111.793, 111.511, 101.229, 58.382, 56.455, 52.594, 46.545 ppm. The protonated 4PBZC <sup>1</sup>H NMR (400 MHz, Deuterium Oxide):  $\delta$  7.67 (d,  $J$  = 9.2 Hz, 1H), 7.28 (dd,  $J$  = 6.4, 6 Hz, 2H), 7.18 (dd,  $J$  = 6.4, 6 Hz, 2H), 6.92 (dd,  $J$  = 11.2, 11.2 Hz, 1H), 6.44 (s, 1H), 6.0 (s, 1H) 3.79–3.77 (m, 4H), 3.76 (s, 3H), 3.41–3.38 (m, 4H). The structure in Scheme 1 was confirmed by FT-IR and MS (see the Supporting Information).

**4.3. Experimental Measurements and Instrumentation.** <sup>1</sup>H NMR spectra were processed on a Varian 400 MHz spectrometer ([www.varian.com](http://www.varian.com)). The pD assessments of the samples were balanced ( $\pm 0.2$  units) by including sufficient

proportions of DCl or NaOD and recorded utilizing a WTW 330i with a WTW Sen Tix Mic glass anode ([www.xylenanalytics.com](http://www.xylenanalytics.com)). The UV–visible absorption spectra and emission spectra were measured on an FSS spectrofluorometer (Edinburgh Instrument Ltd, Livingston, UK, [www.edinst.com](http://www.edinst.com)) at room temperature between 200 and 700 nm for UV–visible and 390–700 nm for fluorescence spectra. The excitation and emission monochromator slit width was set to 2 nm, except in any case indicated otherwise. The pH esteems were recorded utilizing a pH meter (WTW 300i furnished with a WTW Sen Tix Mic Glass terminal). A quartz cuvette (1 cm, 4.0 mL) was utilized in all spectroscopic estimations and was acquired from Starna Cell Inc. (Atascadero, CA, USA) (see the [Supporting Information](#) for details on the procedures for determination of  $pK_a$  values).

**4.4. Competitive Displacement Studies.** The interaction of CAR with the complex of 4PBZC and CB7 was studied by weighing a calculated amount of CAR and dissolving in the stock solution of 4PBZC/CB7 to form 150  $\mu\text{M}$  CAR (see the [Supporting Information](#) for details on the procedures and equation for determination of 1:1 and 2:1 binding affinities). This solution was added gradually to 2.4 mL of 4PBZC/CB7 inclusion complex in the quartz cuvette, followed by the estimation of the absorption and photoluminescence spectra upon each addition of CAR-contained solution (in  $\mu\text{L}$ ). The pH of all solutions remains the same throughout the analysis, and experiments were carried out at room temperature.<sup>42</sup>

**4.5. Sensitivity of the 4PBZC/CB7 Sensor.** The sensor affectability or sensibility was controlled by estimating the fluorescence reaction of the complex of 4PBZC and CB7 at various concentrations of CAR. 1600  $\mu\text{L}$  of CAR solution (prepared in the 4PBZC/CB7 stock solution) was included gradually to 4PBZC/CB7 (2400  $\mu\text{L}$ ), which was then positioned on the fluorescence cuvette quartz. The alignment/calibration curve was obtained by plotting the realized concentration against the maximum intensity of every addition at 430 nm. In determining the LOD, the emission intensity of a free 4PBZC/CB7 solution was measured multiple times to decide the standard deviation, which was increased by 3 and divided by the incline value obtained (slope) from the alignment/calibration curve (slope =  $-2 \times 10^{10}$ ). With respect to other analytical parameters, we have included the limit of quantification, which is equivalent to the standard deviation of 20 clear/free estimations duplicated by 10 and further partitioned by the gradient (slope) of the standard adjustment/calibration curve ranging from 0 to 1000  $\mu\text{L}$ .

**4.6. DFT Calculations.** All calculations were performed with Gaussian 09.<sup>38</sup> The ground-state geometries were optimized using density functional theory, DFT, in the gas phase. The M06-2X method was used for the full optimization with the 6-31G\* basis set. Minima of the calculated structures were characterized by the absence of imaginary frequencies. The calculations for the HOMO and LUMO frontier orbital energies were obtained using time-dependent-DFT at the M06-2X/6-311++G\*\* level of theory.

## ■ ASSOCIATED CONTENT

### SI Supporting Information

The Supporting Information is available free of charge at <https://pubs.acs.org/doi/10.1021/acsomega.1c06287>.

pH titrations; UV–visible absorption binding titrations; NMR binding titrations; fluorescence binding titrations; DFT calculations; and spectral characterization of 4PBZC (PDF)

## ■ AUTHOR INFORMATION

### Corresponding Author

Na'il Saleh – Department of Chemistry, College of Science, United Arab Emirates University, Al Ain 15551, United Arab Emirates; [orcid.org/0000-0003-3282-1156](https://orcid.org/0000-0003-3282-1156); Phone: +971-(0)3-713-6138; Email: [n.saleh@uaeu.ac.ae](mailto:n.saleh@uaeu.ac.ae)

### Authors

Rukayat S. Bojesomo – Department of Chemistry, College of Science, United Arab Emirates University, Al Ain 15551, United Arab Emirates

Khaleel I. Assaf – Department of Chemistry, Faculty of Science, Al-Balqa Applied University, Al-Salt 19117, Jordan; [orcid.org/0000-0003-4331-8492](https://orcid.org/0000-0003-4331-8492)

Haythem A. Saadeh – Department of Chemistry, College of Science, United Arab Emirates University, Al Ain 15551, United Arab Emirates; Department of Chemistry, School of Science, The University of Jordan, Amman 11942, Jordan

Lamia A. Siddig – Department of Chemistry, College of Science, United Arab Emirates University, Al Ain 15551, United Arab Emirates

Complete contact information is available at:

<https://pubs.acs.org/10.1021/acsomega.1c06287>

### Author Contributions

Preparation and characterization of 4PBZC, L.A. and H.S.; theoretical analysis and writing—original draft preparation, K.I.A.; all other experimental analysis and writing—original draft preparation, R.B.; conceptualization, methodology, data curation, writing—review and editing, supervision, and project administration, N.S.; and funding acquisition, N.S. and H.S. All authors have read and agreed to the published version of the article.

### Notes

The authors declare no competing financial interest.

## ■ ACKNOWLEDGMENTS

We thank the research program in United Arab Emirates University for financial grant number UPAR (2020) 31S392.

## ■ REFERENCES

- (1) Nguyen, B. T.; Anslyn, E. V. Indicator–Displacement Assays. *Coord. Chem. Rev.* **2006**, *250*, 3118–3127.
- (2) Sinn, S.; Biedermann, F. Chemical Sensors Based on Cucurbit[*n*]uril Macrocycles. *Isr. J. Chem.* **2018**, *58*, 357–412.
- (3) Ghale, G.; Nau, W. M. Dynamically Analyte-Responsive Macrocyclic Host–Fluorophore Systems. *Acc. Chem. Res.* **2014**, *47*, 2150–2159.
- (4) Mako, T. L.; Racicot, J. M.; Levine, M. Supramolecular Luminescent Sensors. *Chem. Rev.* **2019**, *119*, 322–477.
- (5) Sinn, S.; Krämer, J.; Biedermann, F. Teaching Old Indicators Even More Tricks: Binding Affinity Measurements with the Guest-Displacement Assay (GDA). *Chem. Commun.* **2020**, *56*, 6620–6623.
- (6) Sinn, S.; Spuling, E.; Bräse, S.; Biedermann, F. Rational Design and Implementation of a Cucurbit[8]uril-Based Indicator-Displacement Assay for Application in Blood Serum. *Chem. Sci.* **2019**, *10*, 6584–6593.
- (7) Dewantari, A. A.; Yongwattana, N.; Payongsri, P.; Seemakhan, S.; Borwornpinyo, S.; Ojida, A.; Wongkongkatap, J. Fluorescence

- Detection of Deoxyadenosine in *Cordyceps* Spp. by Indicator Displacement Assay. *Molecules* **2020**, *25*, 2045.
- (8) Isaacs, L. Stimuli Responsive Systems Constructed Using Cucurbit[n]uril-Type Molecular Containers. *Acc. Chem. Res.* **2014**, *47*, 2052–2062.
- (9) Shan, P.-H.; Zhao, J.; Deng, X.-Y.; Lin, R.-L.; Bian, B.; Tao, Z.; Xiao, X.; Liu, J.-X. Selective Recognition and Determination of Phenylalanine by a Fluorescent Probe Based on Cucurbit[8]uril and Palmatine. *Anal. Chim. Acta* **2020**, *1104*, 164–171.
- (10) Chang, Y.-X.; Zhang, X.-M.; Duan, X.-C.; Liu, F.; Du, L.-M. Supramolecular Interaction of Methotrexate with Cucurbit[7]uril and Analytical Application. *Spectrochim. Acta, Part A* **2017**, *183*, 131–137.
- (11) Zhu, L.; Zhao, Z.; Zhang, X.; Zhang, H.; Liang, F.; Liu, S. A Highly Selective and Strong Anti-Interference Host-Guest Complex as Fluorescent Probe for Detection of Amantadine by Indicator Displacement Assay. *Molecules* **2018**, *23*, 947.
- (12) Du, X.; Hao, H.; Qin, A.; Tang, B. Z. Highly Sensitive Chemosensor for Detection of Methamphetamine by the Combination of AIE Luminogen and Cucurbit[7]uril. *Dyes Pigm.* **2020**, *180*, 108413.
- (13) Nilam, M.; Huang, C.; Karmacharya, S.; Aryal, G. H.; Huang, L.; Nau, W. M.; Assaf, K. I. Host-Guest Complexation Affects Perylene-Based Dye Aggregation. *ChemistrySelect* **2020**, *5*, 5850–5854.
- (14) Liu, Y.; Zhang, Q.; Crespi, S.; Chen, S.; Zhang, X. K.; Xu, T. Y.; Ma, C. S.; Zhou, S. W.; Shi, Z. T.; Tian, H.; Feringa, B. L.; Qu, D. H. Motorized Macrocyclic Host with Switchable and Stereoselective Guest Recognition. *Angew. Chem., Int. Ed.* **2021**, *60*, 16129–16138.
- (15) Hettiarachchi, G.; Nguyen, D.; Wu, J.; Lucas, D.; Ma, D.; Isaacs, L.; Briken, V. Toxicology and Drug Delivery by Cucurbit[n]uril Type Molecular Containers. *PLoS One* **2010**, *5*, No. e10514.
- (16) Uzunova, V. D.; Cullinane, C.; Brix, K.; Nau, W. M.; Day, A. I. Toxicity of Cucurbit[7]uril and Cucurbit[8]uril: An Exploratory in Vitro and in Vivo Study. *Org. Biomol. Chem.* **2010**, *8*, 2037–2042.
- (17) Yin, H.; Wang, Z.; Wang, R. Modulation of Chemical and Biological Properties of Biomedically Relevant Guest Molecules by Cucurbituril-Type Hosts. In *Handbook of Macrocyclic Supramolecular Assembly*; Liu, Y., Chen, Y., Zhang, H.-Y., Eds.; Springer: Singapore, 2019; pp 1–25.
- (18) Yin, H.; Cheng, Q.; Rosas, R.; Viel, S.; Monnier, V.; Charles, L.; Siri, D.; Gigmès, D.; Ouari, O.; Wang, R.; Kermagoret, A.; Bardelang, D. A Cucurbit[8]uril 2:2 Complex with a Negative pK<sub>a</sub> Shift. *Chem.—Eur. J.* **2019**, *25*, 12552–12559.
- (19) Saleh, N.; Al-Soud, Y. A.; Al-Kaabi, L.; Ghosh, I.; Nau, W. M. A Coumarin-Based Fluorescent PET Sensor Utilizing Supramolecular pK<sub>a</sub> Shifts. *Tetrahedron Lett.* **2011**, *52*, 5249–5254.
- (20) Barooah, N.; Mohanty, J.; Pal, H.; Bhasikuttan, A. C. Stimulus-Responsive Supramolecular pK<sub>a</sub> Tuning of Cucurbit[7]uril Encapsulated Coumarin 6 Dye. *J. Phys. Chem. B* **2012**, *116*, 3683–3689.
- (21) Minami, T.; Esipenko, N. A.; Akdeniz, A.; Zhang, B.; Isaacs, L.; Anzenbacher, P. Multianalyte Sensing of Addictive Over-the-Counter (OTC) Drugs. *J. Am. Chem. Soc.* **2013**, *135*, 15238–15243.
- (22) Webber, M. J.; Langer, R. Drug Delivery by Supramolecular Design. *Chem. Soc. Rev.* **2017**, *46*, 6600–6620.
- (23) Chandra, F.; Kumar, P.; Koner, A. L. Encapsulation and Modulation of Protolytic Equilibrium of  $\beta$ -Carboline-Based Nornarmane Drug by Cucurbit[7]uril and Micellar Environments for Enhanced Cellular Uptake. *Colloids Surf., B* **2018**, *171*, 530–537.
- (24) Da Silva, J. P.; Jayaraj, N.; Jockusch, S.; Turro, N. J.; Ramamurthy, V. Aggregates of Cucurbituril Complexes in the Gas Phase. *Org. Lett.* **2011**, *13*, 2410–2413.
- (25) Mallick, S.; Pal, K.; Chandra, F.; Koner, A. L. Investigation of the Effect of Cucurbit[7]uril Complexation on the Photophysical and Acid–Base Properties of the Antimalarial Drug Quinine. *Phys. Chem. Chem. Phys.* **2016**, *18*, 30520–30529.
- (26) Lazar, A. I.; Biedermann, F.; Mustafina, K. R.; Assaf, K. I.; Hennig, A.; Nau, W. M. Nanomolar Binding of Steroids to Cucurbit[n]urils: Selectivity and Applications. *J. Am. Chem. Soc.* **2016**, *138*, 13022–13029.
- (27) Praetorius, A.; Bailey, D. M.; Schwarzlose, T.; Nau, W. M. Design of a Fluorescent Dye for Indicator Displacement from Cucurbiturils: A Macrocyclic-Responsive Fluorescent Switch Operating through a pK<sub>a</sub> Shift. *Org. Lett.* **2008**, *10*, 4089–4092.
- (28) Yin, T.; Zhang, S.; Li, M.; Redshaw, C.; Ni, X.-L. Macrocyclic Encapsulation Triggered Supramolecular pK<sub>a</sub> Shift: A Fluorescence Indicator for Detecting Octreotide in Aqueous Solution. *Sens. Actuators, B* **2019**, *281*, 568–573.
- (29) Vogler, A. V. Balzani and F. Scandola: Supramolecular Photochemistry, aus: Ellis Horwood Series in Physical Chemistry: Photo and Radiation Chemistry, Ellis Horwood, New York, London, Toronto, Sydney, Tokyo, Singapore 1991, ISBN 0-B-877531-1, 427 Seiten. Preis: US Dollar 123.95. *Ber. Bunsen-Ges. Physik. Chem.* **1991**, *95*, 1161–1162.
- (30) Selinger, A. J.; Macartney, D. H. Cucurbit[7]uril Complexations of Good's Buffers. *RSC Adv.* **2017**, *7*, 42513–42518.
- (31) Wang, R.; Bardelang, D.; Waite, M.; Udachin, K. A.; Leek, D. M.; Yu, K.; Ratcliffe, C. I.; Ripmeester, J. A. Inclusion Complexes of Coumarin in Cucurbiturils. *Org. Biomol. Chem.* **2009**, *7*, 2435.
- (32) Horak, E.; Kassal, P.; Murković Steinberg, I. Benzimidazole as a Structural Unit in Fluorescent Chemical Sensors: The Hidden Properties of a Multifunctional Heterocyclic Scaffold. *Supramol. Chem.* **2018**, *30*, 838–857.
- (33) Chen, S.-H.; Jiang, K.; Xiao, Y.; Cao, X.-Y.; Arulkumar, M.; Wang, Z.-Y. Recent Endeavors on Design, Synthesis, Fluorescence Mechanisms and Applications of Benzazole-Based Molecular Probes toward Miscellaneous Species. *Dyes Pigm.* **2020**, *175*, 108157.
- (34) Lazar, A. I.; Rohacova, J.; Nau, W. M. Comparison of Complexation-Induced pK<sub>a</sub> Shifts in the Ground and Excited States of Dyes as Well as Different Macrocyclic Hosts and Their Manifestation in Host-Retarded Excited-Dye Deprotonation. *J. Phys. Chem. B* **2017**, *121*, 11390–11398.
- (35) Birtić, S.; Dussort, P.; Pierre, F.-X.; Bily, A. C.; Roller, M. Carnosic Acid. *Phytochemistry* **2015**, *115*, 9–19.
- (36) Alsamri, H.; El Hasasna, H.; Al Dhaheri, Y.; Eid, A. H.; Attoub, S.; Iratni, R. Carnosol, a Natural Polyphenol, Inhibits Migration, Metastasis, and Tumor Growth of Breast Cancer via a ROS-Dependent Proteasome Degradation of STAT3. *Front. Oncol.* **2019**, *9*, 743.
- (37) Cerón-Carrasco, J. P.; den-Haan, H.; Peña-García, J.; Contreras-García, J.; Pérez-Sánchez, H. Exploiting the Cyclodextrins Ability for Antioxidants Encapsulation: A Computational Approach to Carnosol and Carnosic Acid Embedding. *Comput. Theor. Chem.* **2016**, *1077*, 65–73.
- (38) Park, J.; Rho, S.-J.; Kim, Y.-R. Enhancing Antioxidant and Antimicrobial Activity of Carnosic Acid in Rosemary (*Rosmarinus Officinalis* L.) Extract by Complexation with Cyclic Glucans. *Food Chem.* **2019**, *299*, 125119.
- (39) Li, Y.; Li, C.-F.; Du, L.-M.; Feng, J.-X.; Liu, H.-L.; Fu, Y.-L. A Competitive Strategy Based on Cucurbit[7]uril Supramolecular Interaction for Simple and Sensitive Detection of Dibucaine. *Talanta* **2015**, *132*, 653–657.
- (40) Liu, H.; Fang, G.; Deng, Q.; Wang, S. A Triple-Dimensional Sensing Chip for Discrimination of Eight Antioxidants Based on Quantum Dots and Graphene. *Biosens. Bioelectron.* **2015**, *74*, 313–317.
- (41) Yin, T.; Zhang, S.; Li, M.; Redshaw, C.; Ni, X.-L. Macrocyclic Encapsulation Triggered Supramolecular pK<sub>a</sub> Shift: A Fluorescence Indicator for Detecting Octreotide in Aqueous Solution. *Sens. Actuators, B* **2019**, *281*, 568–573.
- (42) Saleh, N.; Al-handawi, M. B.; Bufarousha, M. S.; Assaf, K. I.; Nau, W. M. Tuning Protonation States of Tripeleppamine Antihistamines by Cucurbit[7]uril. *J. Phys. Org. Chem.* **2016**, *29*, 101–106.